KU LEUVEN

Dynamic and structural investigation of capillary suspensions

IFPRI Annual Meeting 2022

Jens Allard and Erin Koos

KU Leuven
Department of Chemical Engineering
Section Soft Matter, Rheology and Technology

Hello and thank you for listening to (reading) this online version of our presentation at the IFPRI Annual Meeting 2022.

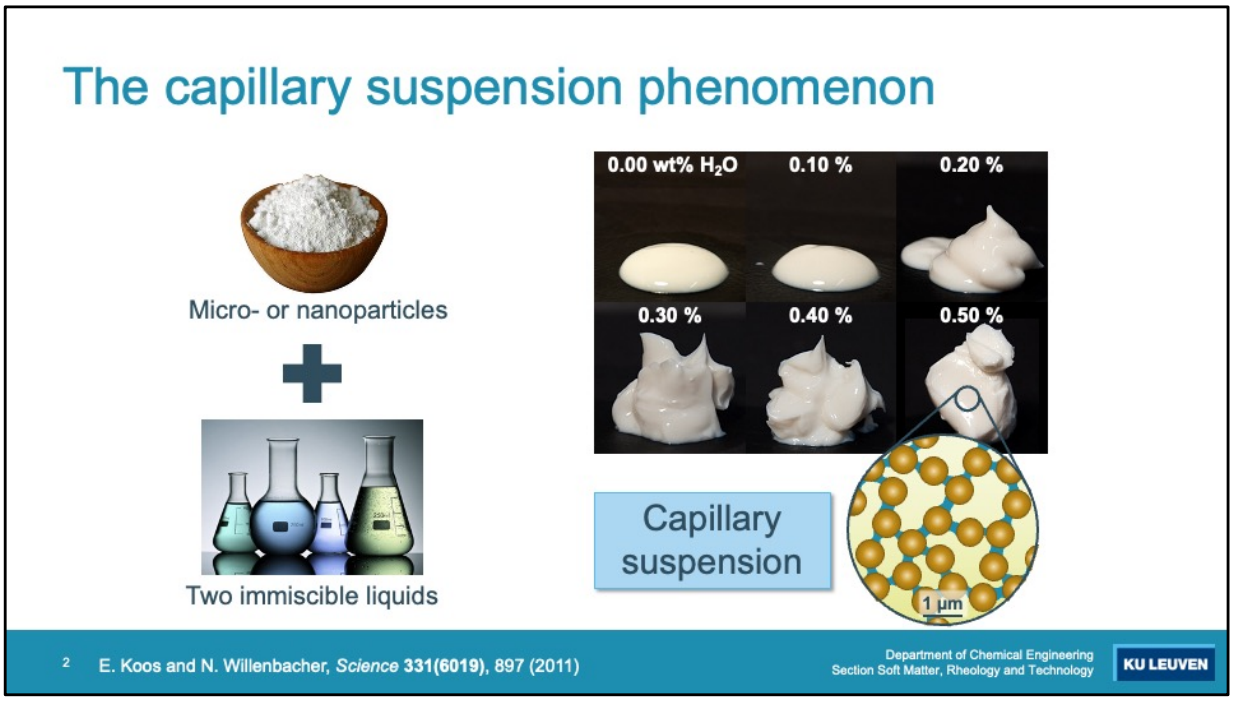

To start, let us quickly remind you about capillary suspensions. Capillary suspensions are solid-liquid-liquid systems, typically formed when a small amount of a secondary liquid is added to a suspension of micro- or nanoparticles. The two liquids must be (partial) immiscible and the secondary fluid is often present in only a few percent. This secondary liquid leads to the formation of a sample-spanning particle network caused by the capillary attraction between the particles. This is like the addition of small amounts of water to the grains of sand in a sandcastle, but here our grains are much smaller, the air is replaced by a liquid, and we usually have a much lower particle loading.

As can be seen in the example on the right, a dramatic change in the bulk properties of the materials occurs with very small amounts of liquid. In this case, using a suspension of calcium carbonate in an oil with small amounts of water, less than 0.5% water by weight increases the yield stress and viscosity by several orders of magnitude.

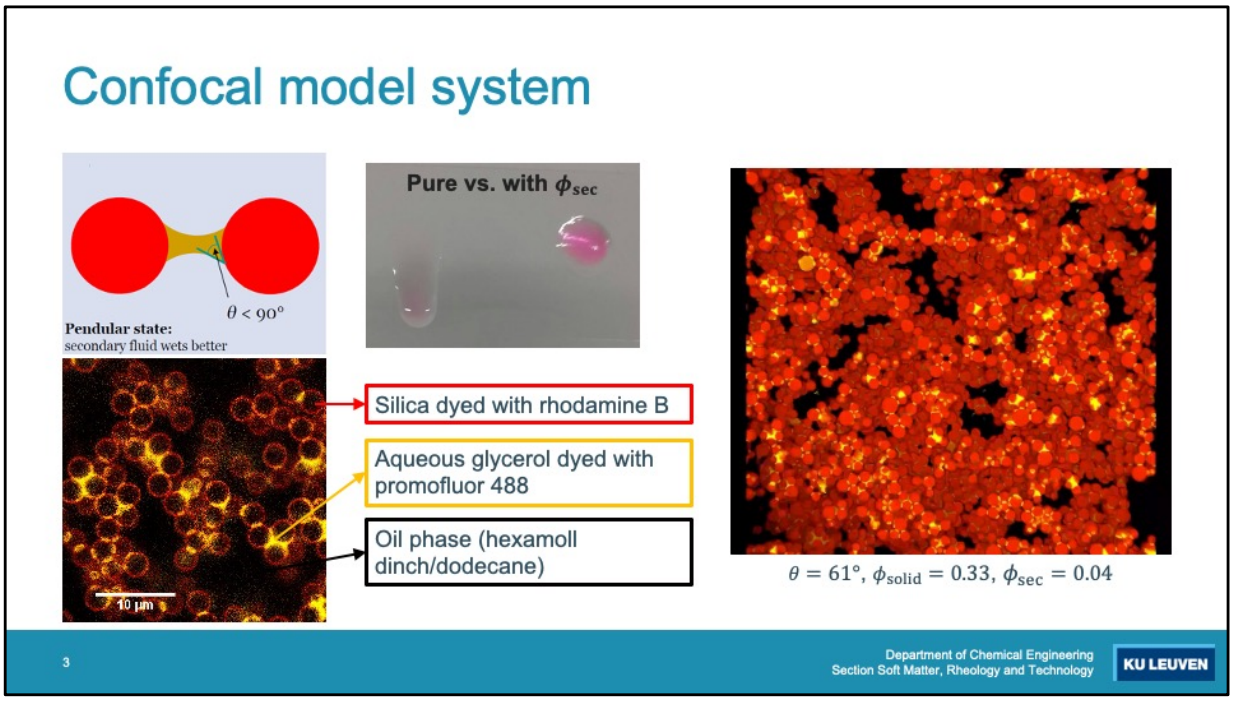

To investigate the structure of these networks, we use a confocal model system composed of silica particles dyed with rhodamine B isothiocyanate. Porous particles are dyed uniformly throughout their interior (as shown here in red) and nonporous particles are only dyed on the surface (visible later as rings). The aqueous phase, which is usually the secondary phase in these experiments, is a mixture of water and glycerol dyed with promofluor 488 (shown here in yellow). The oil phase is undyed and appears black on the images. Without secondary liquid, the pure suspension freely flows (upper right image) whereas it shows gel-like properties with a volume of added secondary liquid ϕ_{sec}. By using silica particles, we can change the three-phase contact angle θ through silanization. This lets us switch between the pendular state $\theta < 90°$ where the secondary liquid preferentially wets the particles, forming binary bridges between the particles, and the capillary state $\theta > 90°$ where the particles from small clusters surrounding the secondary liquid droplets.

This index-matched system is applicable to both confocal microscopy and can also be used for simple rheological measurements. We have carefully controlled the mixing procedure to ensure that the samples are uniform. Thus, the structure should be identical throughout the sample volume and we won't make mistakes by inferring changes in the material structure when it is only an error caused by the sampling location. Furthermore, we can tune the sample properties: the ratio of the three components and the contact angle.

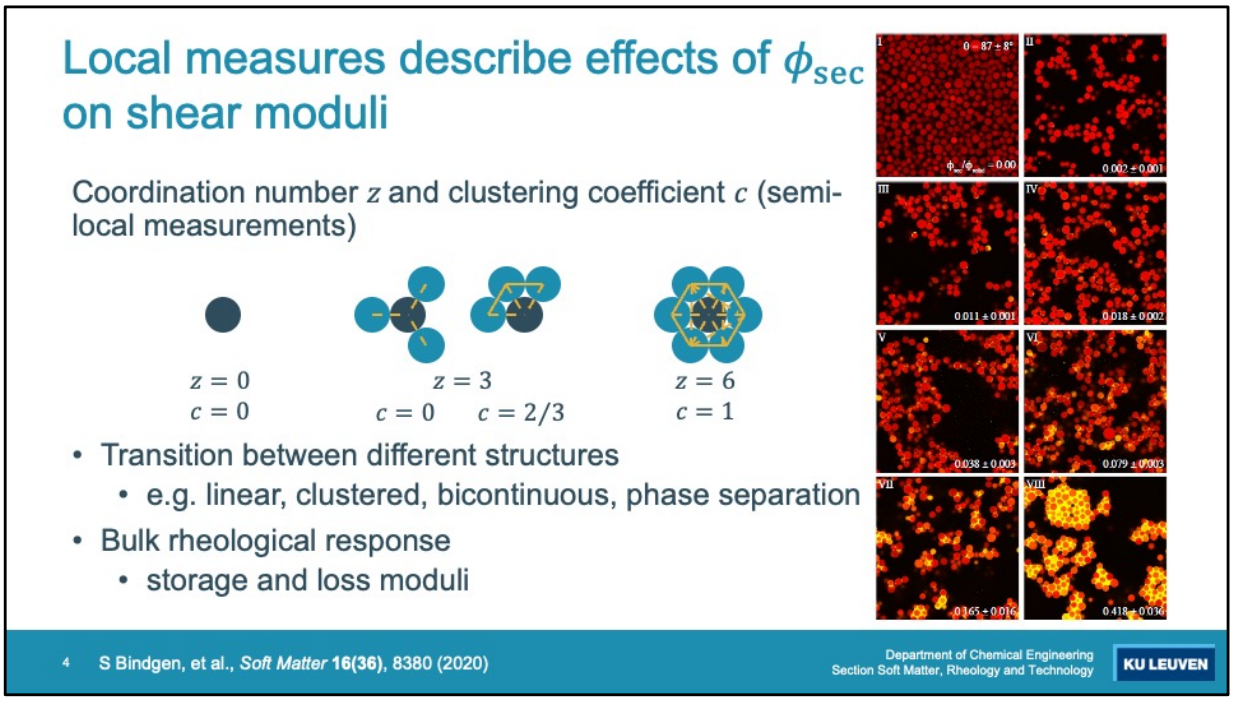

To characterize the particle networks, we can use both local and global measures. Since network-level measures, such as the fractal dimensionality, are ill-suited to dense and heterogeneous networks (as we have here), we prefer using the semi-local measures.

The number of neighbors, the coordination number z, which can be readily calculated from confocal images, provides some insights, but has a tenuous link to rheology. We therefore supplement this measure with another measure from graph theory, namely the clustering coefficient, as shown in the sketch. The local clustering coefficient is defined as

$$c = \frac{2e}{z(z-1)}$$

where the number of bonds between neighbors (dashed lines) is z and the connections between these neighbors (solid lines) is e. An alternative definition of the clustering coefficient can be achieved by counting the number of triangles through a node (particle) compared to the number of neighbors. As illustrated in the sketch intermediate coordination numbers can either have low clustering ($c \to 0$) or high clustering ($c \to 1$) with clear implications of the mechanical response of the cluster. Although the upper limit of the clustering coefficient is $c = 1$, as shown in the non-physical packed structure on the left, real, e.g., biological networks, almost never reach this limit and $c > 0.5$ is considered as high clustering.

As shown in our Soft Matter paper, these measures are able to capture transitions

between the different microstructures (pendular, funicular, bicontinuous) and can help us predict the rheological properties.

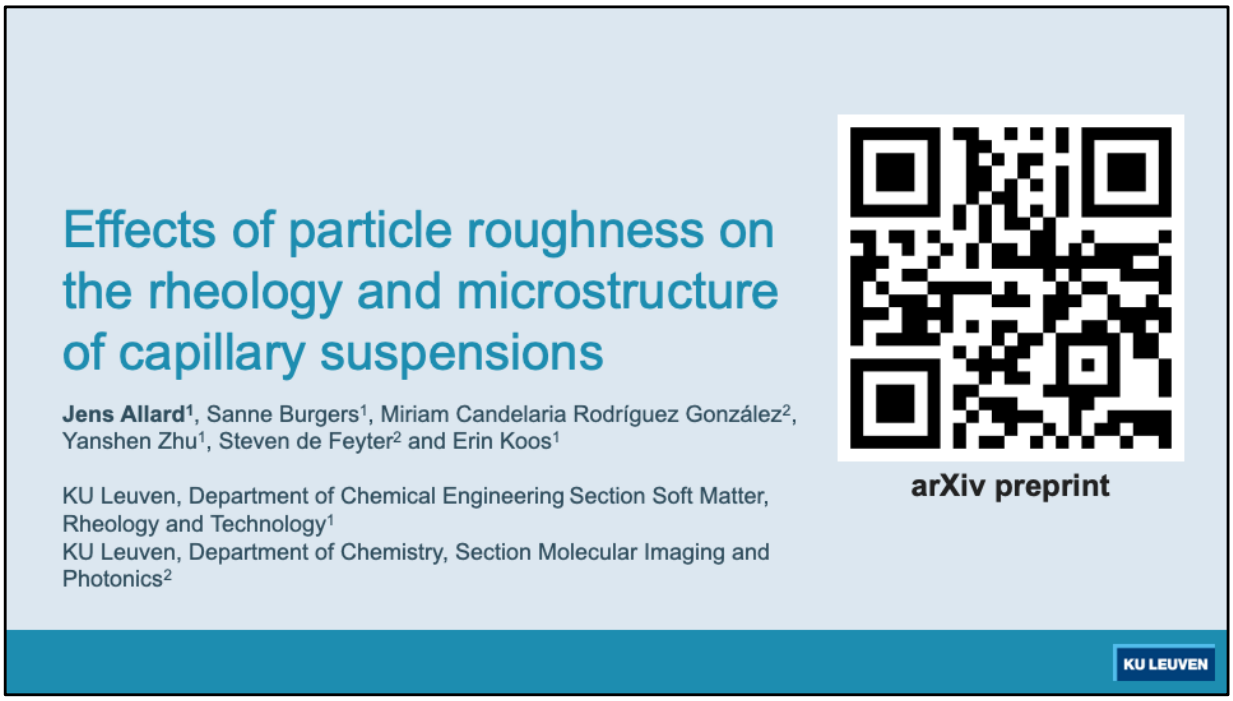

Work this year was split between finishing the work on particle roughness and other projects. The paper "Effects of particle roughness on the rheology and microstructure of capillary suspensions" has been published by *Colloids and Surfaces A* (https://doi.org/10.1016/j.colsurfa.2022.129224) and is freely available on arXiv (https://arxiv.org/abs/2203.07779).

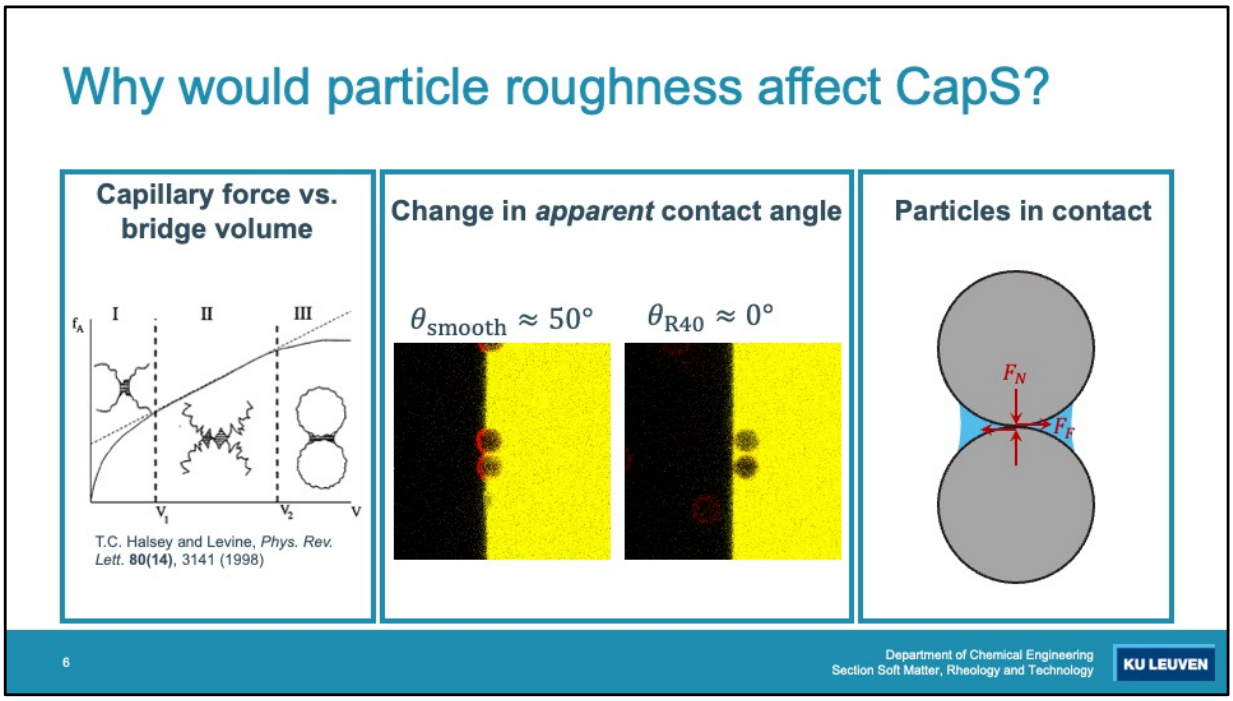

We expect the particle roughness to affect capillary suspensions in three ways:

1. The bridging fluid may be trapped in troughs caused by the roughness. With equal volumes of added secondary fluid, we expect increasing roughness to reduce the effective bridge size between neighboring particles. This will transition the system from the spherical regime (type III) for smooth particles towards either the roughness (type II) or asperity (type I) regimes with increasing roughness. The decrease in the effective bridge volume should result in a decrease in the network strength (as measured via the shear modulus G' or yield stress σ_y).
2. The particle roughness may result in a change in the apparent contact angle. For homogeneous wetting of the asperities (Wenzel wetting), the contact angle change would be given by $\cos(\theta_{\mathrm{rough}}) = r_w \cos(\theta_{\mathrm{smooth}})$, where θ is the contact angle of the bridging fluid and r_w is the ratio of the total surface area and projected surface area. In the example images, the difference between smooth particles and particles with a slight roughness are shown. Here, the particles are pre-dispersed in the bulk liquid (black) and migrated towards the liquid-liquid interface, which means an advancing contact angle was measured as this best mimics the sample preparation conditions. This difference between the contact angles is consistent with Wenzel wetting for a roughness factor of $r_w = 1.9$ (sphere covered by closely-packed asperities). Increased roughness may also contribute to a larger contact angle hysteresis and contact line pinning.
3. Finally, particles in contact exhibit a (small) fictional contribution caused by the superposition of the attractive capillary force and repulsive Hertzian contact. Increased roughness can modify both the magnitude of the frictional dissipation

and possibly even the type of friction observed.

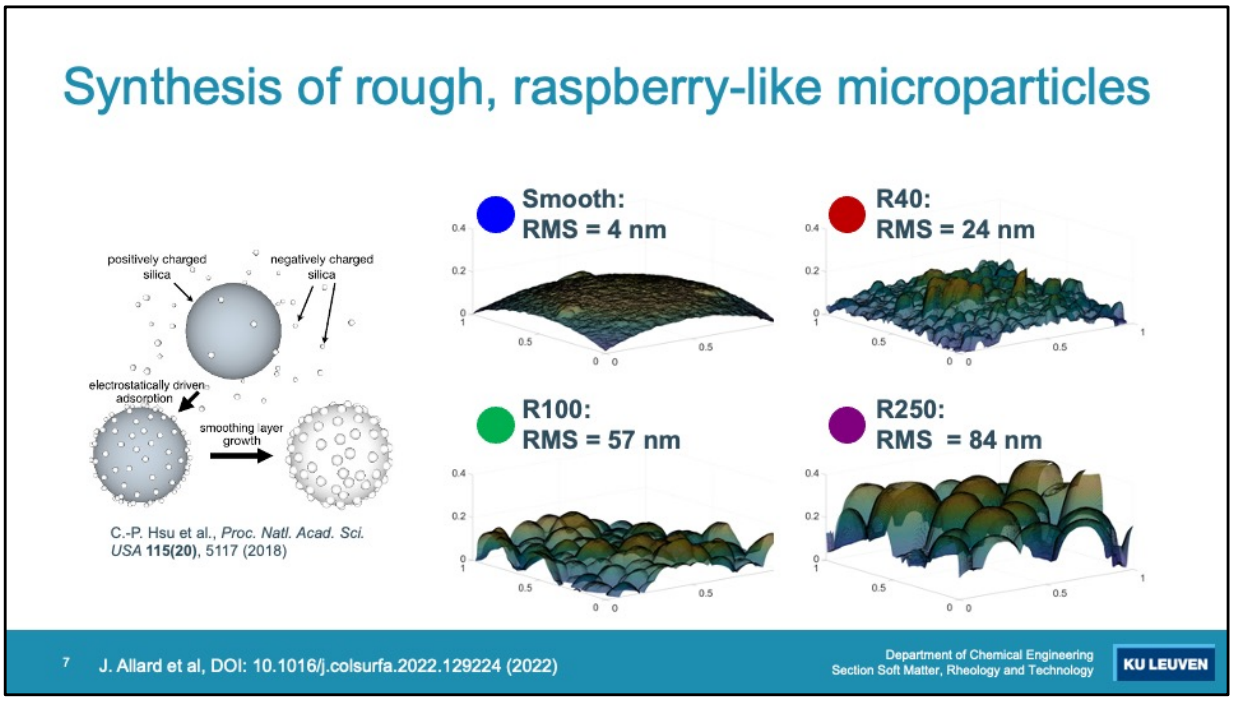

To directly test the influence of particle roughness on our system, we follow the formulation of C.-P. Hsu et al. where silica nanoparticles are electrostatically adsorbed onto the surface of the larger microparticles and then smoothed with a Stöber silica layer. The particles are uniformly covered by nanoparticles and with increasing nanoparticle size, the curvature-corrected final asperity height and root mean squared (RMS) roughness increase accordingly. In the example shown on the right, we attached 40 nm silica nanoparticles onto the surface of the 3 µm microparticles, resulting in an RMS roughness of 23 nm as measured using AFM.

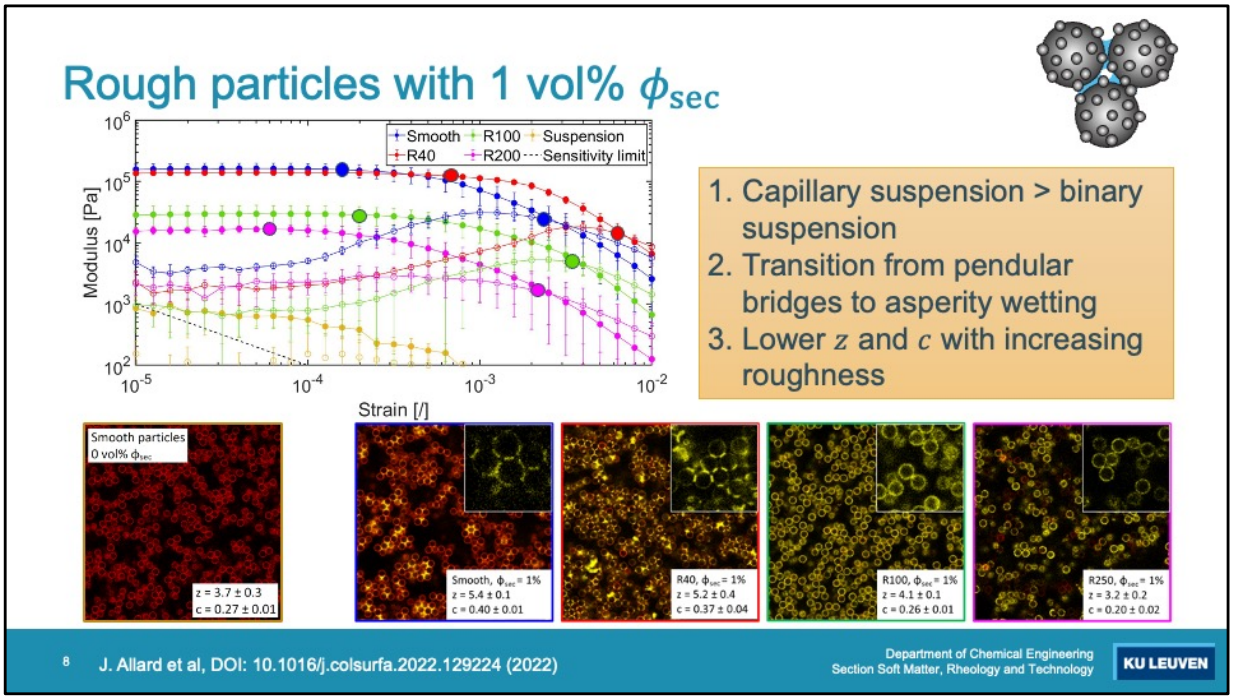

To characterize the samples, we used both oscillatory amplitude sweeps on a rheometer and characterized the structure using a confocal microscope. The smooth particle sample, without added secondary liquid, has a weak van der Waals network with low critical strain. Adding $\phi_{sec} = 1$ vol% of secondary liquid significantly increases the shear moduli regardless of the particle roughness. All capillary suspensions show an increase of 1 or 2 decades in plateau storage modulus. The high roughness samples, R100 and R250, have significantly lower moduli compared to the smooth and R40 particles. The R40 capillary suspension has a nearly identical plateau storage modulus ($G_0 = 1.4 \times 10^5$ Pa) as the smooth particle suspension ($G_0 = 1.6 \times 10^5$ Pa), but longer linear viscoelastic (LVE) region. The R250 sample has a shorter LVE region ($\gamma_{crit} = 1.3 \times 10^{-4}$) compared to the smooth ($\gamma_{crit} = 1.8 \times 10^{-4}$). Interestingly, the R100 sample already has a slightly longer LVE region ($\gamma_{crit} = 2.6 \times 10^{-4}$) even though the G', which suggests that the roughness influences the critical strain. The decrease in G' is accompanied by a simultaneous increase in G''.

The coordination number and clustering coefficient also increases relative to the $\phi_{sec} = 0$ vol% case for all samples except R250. Both z and c decrease with increasing roughness. The reason for this change is that the secondary liquid volume is not sufficient to completely fill the asperities, preventing the formation of a single pendular bridge (spherical regime). This situation, where only small capillary bridges between the asperities are formed (asperity or roughness regime), results in a weaker capillary force than for a pendular bridge. The lower interparticle force explains why the shear moduli of the high roughness suspensions are lower relative to the smooth

particles. To account for this shift in the wetting regime, we can adjust the secondary fluid content.

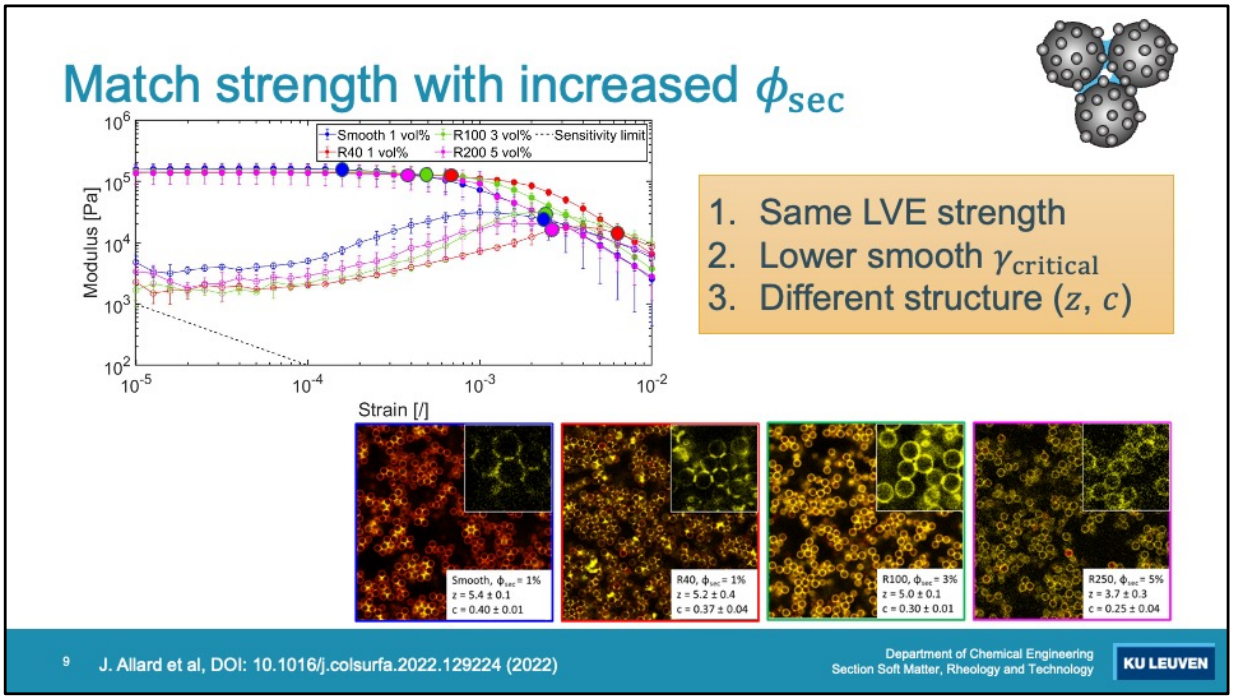

By adjusting the secondary fluid volume for the high roughness samples, the storage modulus in all samples can be matched. To do this, we simply added the extra volume needed to fill the asperities, which resulted in a composition with $\phi_{sec} = 3$ vol% for R100 and $\phi_{sec} = 5$ vol% for R250. After the addition of the extra liquid, these two samples also show toroidal bridges on the confocal micrographs. There remains, however, an increase in the critical strain, i.e., the end of the LVE region, for all rough samples compared to the smooth sample. The peak in the loss modulus also appears at lower strain for the smooth particles.

The increased yield strain for all three rough samples ($\gamma_{crit} = 2.3 \times 10^{-4}$ to 3.7×10^{-4}) compared to the smooth particle system ($\gamma_{crit} = 1.8 \times 10^{-4}$) must therefore be due to the physical presence of the roughness. If the yield stress is evaluated as the stress at the end of the LVE region, the rough particles have a higher yield stress ($\sigma_y \approx 41 - 54$ Pa) than the smooth particle system ($\sigma_y \approx 31$ Pa) due to their higher yield strain. The increased strength can be caused by an additional frictional contribution due to the roughness (that is a tangential contact force due to interlocking asperities) on top of the capillary force that has to be overcome before particle-particle movement can occur.

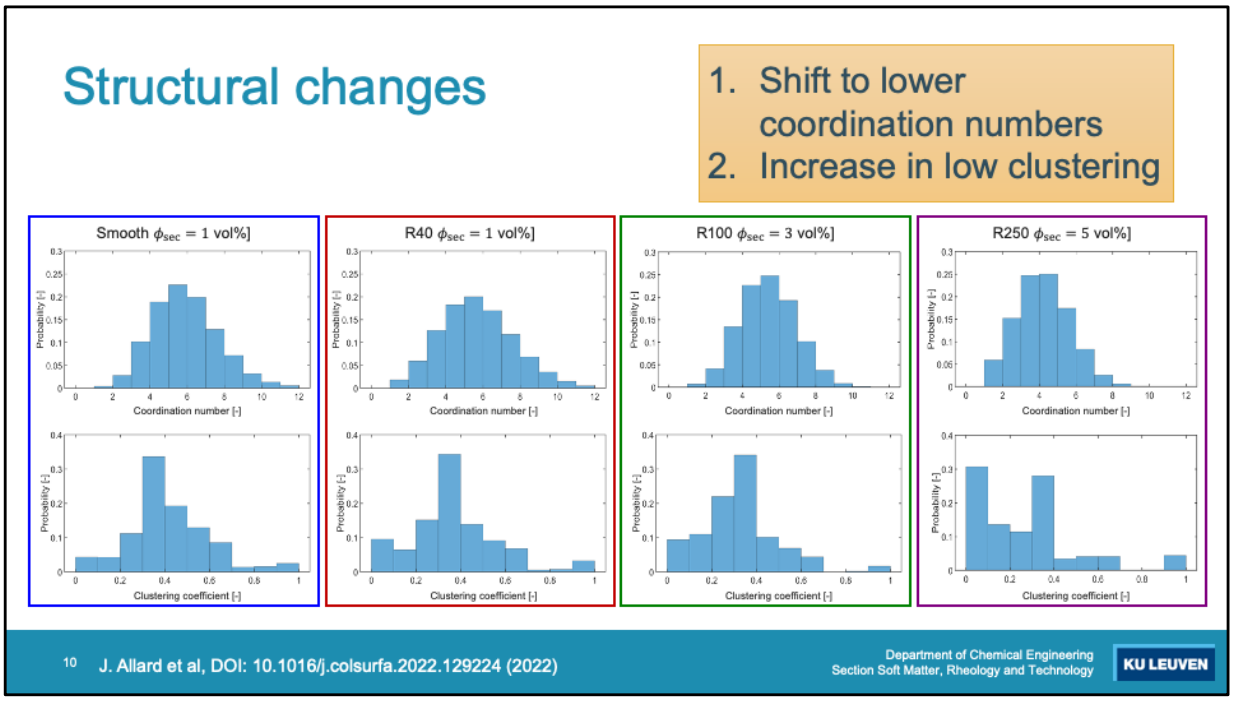

The trend of a decrease in the average coordination number and clustering coefficient with increasing roughness also prevails for the adjusted R100 and R250 samples. This is also visible in the probability distributions. These histograms show the distributions behind the mean coordination numbers and clustering coefficients. With increased particle roughness, the entire coordination number distribution shifts to lower values and the high coordination number tail disappears. For the R250 sample, a large increase in $z = 1$ and $z = 2$ can be seen. For the clustering coefficient, there is a gradual increase in $c < 0.2$ with a simultaneous decrease in $c > 0.4$. For the R250 sample, we see a sharp increase of $c = 0$ partially caused by the shift towards linear strings or small branches with one or two neighbors. The absence of high coordination number and clustering coefficient values implies that no large particle aggregates are formed during the suspension preparation phase when a large secondary liquid droplet is present. For the rough particles, more secondary liquid is used to fill the asperities, which decreases the chance of a local excess of secondary liquid during the mixing process.

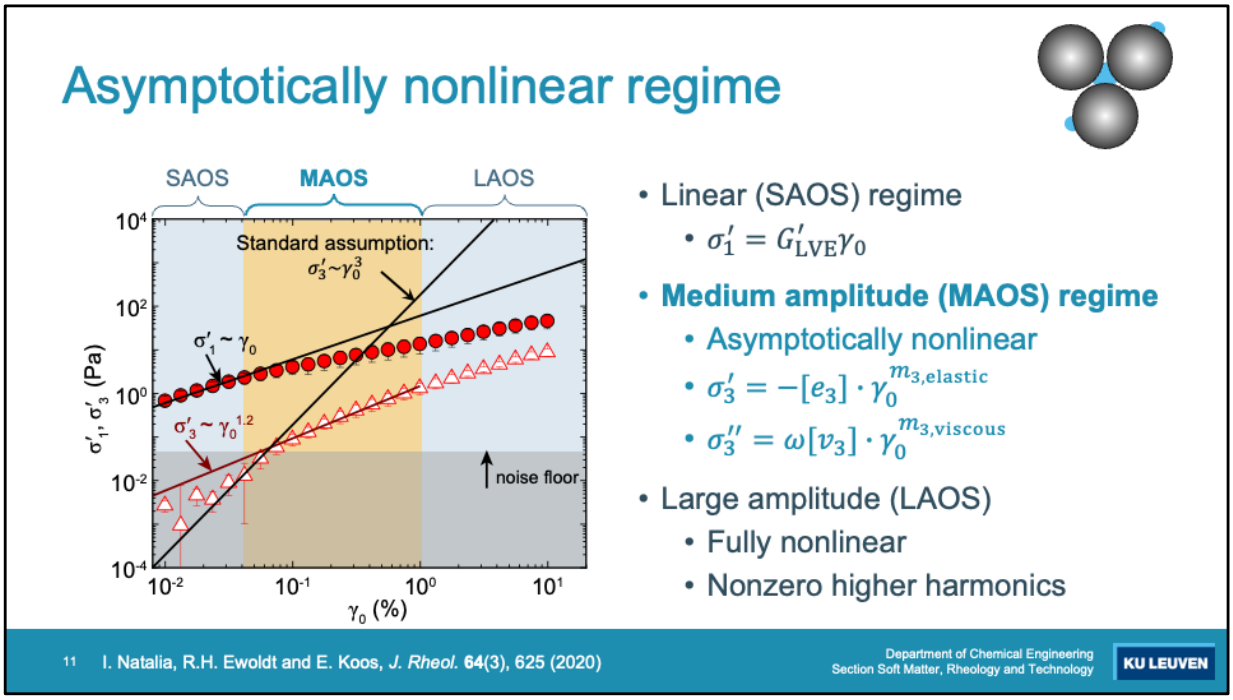

To capture changes in the particle interactions, the influence of particle roughness was examined using information obtained from the medium amplitude (or asymptotically nonlinear) oscillatory shear regime (MAOS). By definition, the MAOS regime is the nonlinear region where only the first and third harmonic stress signals appear. Previous research has shown that the scaling of the third harmonic is non-integer and non-cubic ($\sigma_3 \sim \gamma_0^{m_3}$, $m_3 \neq 3$) and that it is sensitive to particle collisions. Since the particle collisions are expected to be indirectly affected by the roughness through the strength of the bridges and directly affected via the frictional interactions, the third harmonic elastic (σ'_3) and viscous (σ''_3) response should vary between the smooth and rough particles.

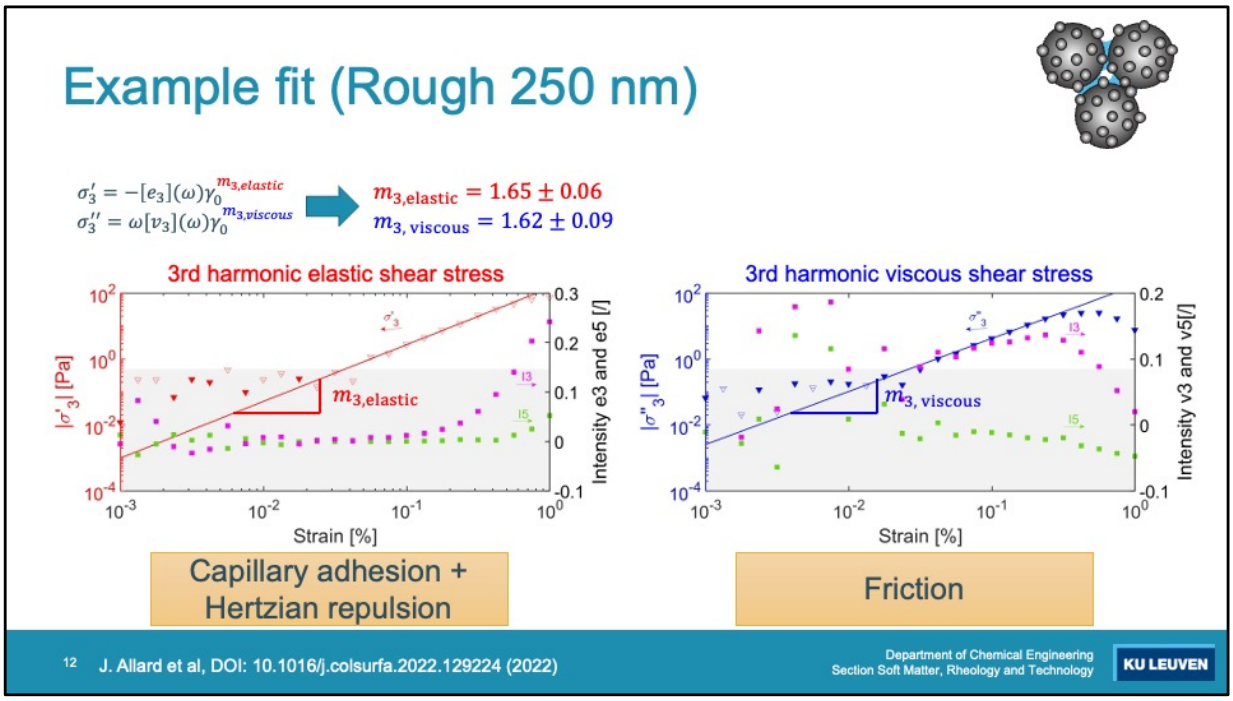

One example fit of the power law scaling for the R250 sample with adjusted secondary liquid volume ($\phi_{sec} = 5$ vol%) is shown here. The the third harmonics σ'_3 (left, red) and σ''_3 (right, blue), are plotted as a function of strain together with the intensity of the third and fifth harmonics. The power law slopes $m_{3,\text{elastic}}$ and $m_{3,\text{viscous}}$ are determined from the power law fit with a fitting region taken as the strain values between the noise floor and the maximum of the third harmonic viscous intensity. The magnitude of the fifth harmonic, σ_5/σ_1, should be negligibly small in this region. As can be seen on the right the viscous intensity σ''_5/σ''_1 remains small while the elastic fifth harmonic σ'_5/σ'_1 only begins to rise near the end of the fitting region.

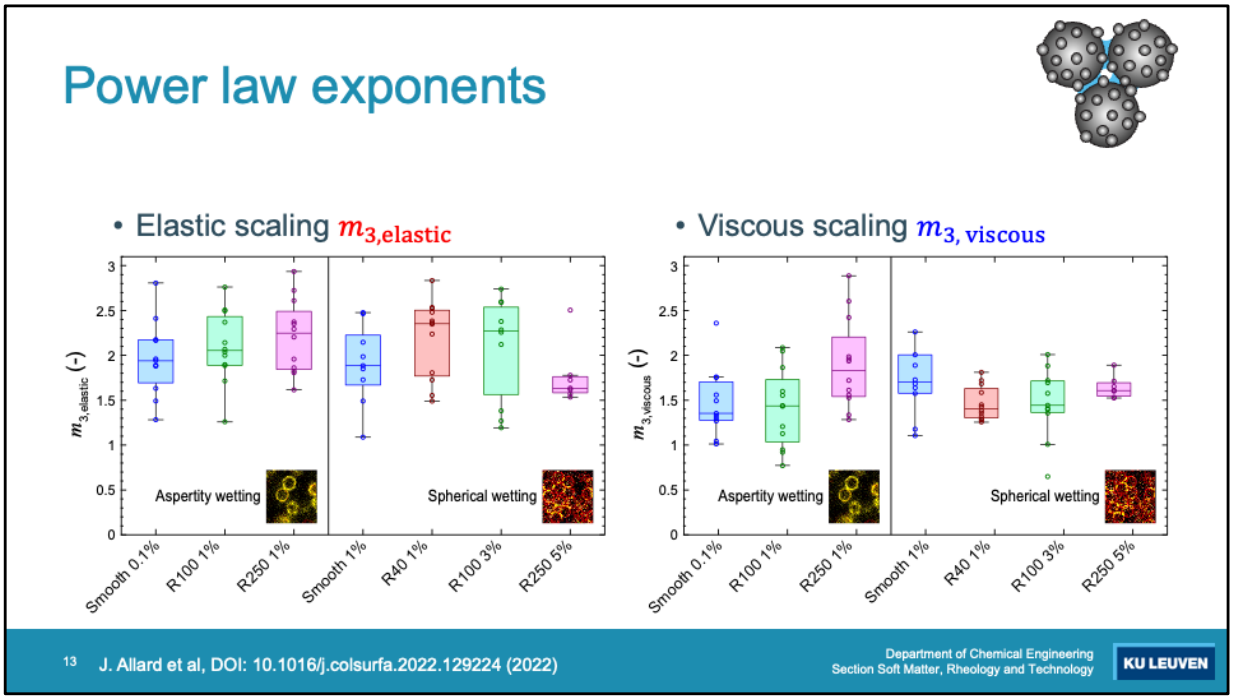

The results of the power law fitting of σ'_3 and σ''_3 for both the samples with $\phi_{sec} =$ 1 vol% and adjusted secondary fluid is shown here. First, both the scaling of $m_{3,\mathrm{elastic}}$ and $m_{3,\mathrm{viscous}}$ is noncubic and noninteger for all samples, in accordance with the works of Natalia et al. (The power law exponents do not differ significantly between sample groups, with $m_{3,\mathrm{elastic}}$ values falling mostly between 1.5 and 2.5 and $m_{3,\mathrm{viscous}}$ values between 1 and 2.

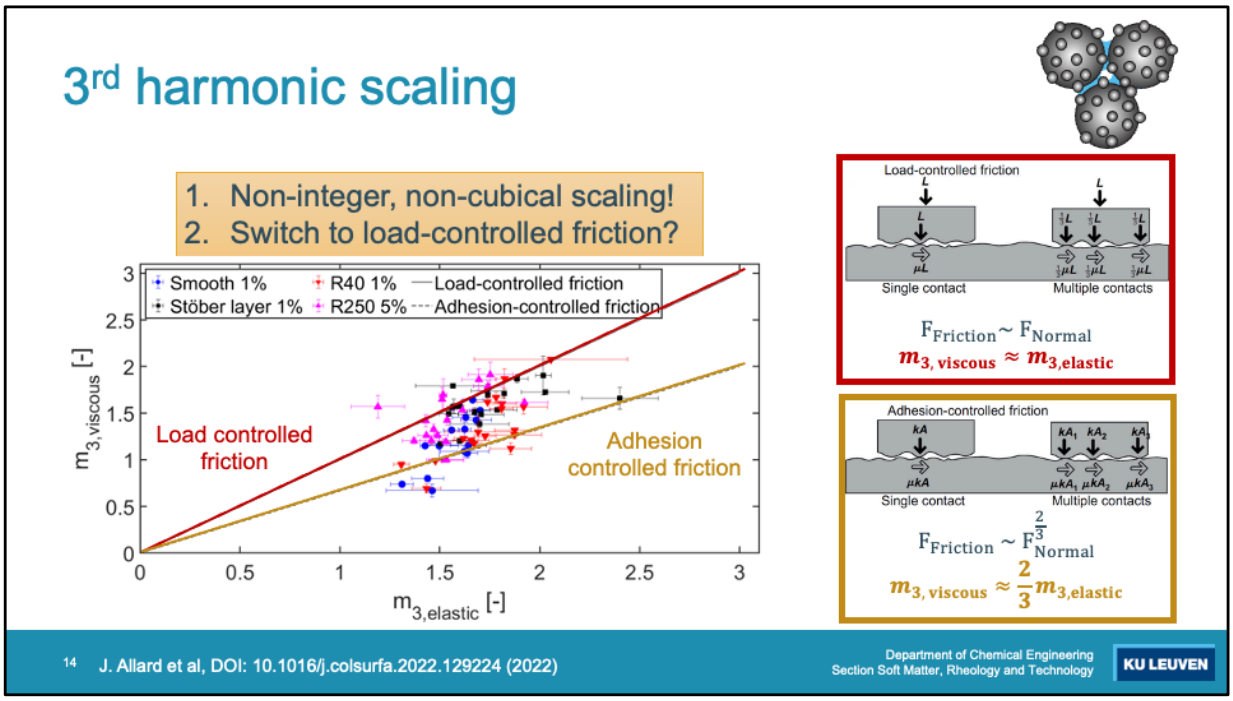

The viscous scaling should be related to dissipative frictional contacts in the system. For low normal forces and few contacting asperities, Hertzian contact theory predicts an elastic deformation of the asperities leading to a friction force $F_{Friction} \sim F_{Normal}^{\frac{2}{3}}$, also known as adhesion-controlled friction. In case of a high normal force or many asperities, Amonton's law applies leading to load-controlled friction with $F_{Friction} \sim F_{Normal}$. For capillary suspensions, the normal force is given by the capillary bridge force combined with the influence of the applied deformation. This leads to a relationship between the elastic and viscous third harmonic power law scalings with either $m_{3,\,viscous} \approx m_{3,elastic}$ for load-controlled friction, or $m_{3,\,viscous} \approx \frac{2}{3} m_{3,elastic}$ for adhesion-controlled friction.

No sample exhibits purely load- or adhesion-controlled behavior and most points are situated in between the two diagonals, even for the smooth particles. The switch to Stöber covered smooth particles resulted in a slight increase in $m_{3,viscous}/m_{3,elastic}$ towards unity. This is in contrast to the results of Natalia et al. (where the adhesion-controlled friction dominated. However, a Student's t-test with a 95 % confidence interval shows that the smooth particle data could come from the adhesion-controlled scaling (p-value = 0.052), whereas the R250 sample could come from the load-controlled scaling (p-value = 0.105), indicating a possible switch to load-controlled friction for rough particles where multiple asperities are in contact.

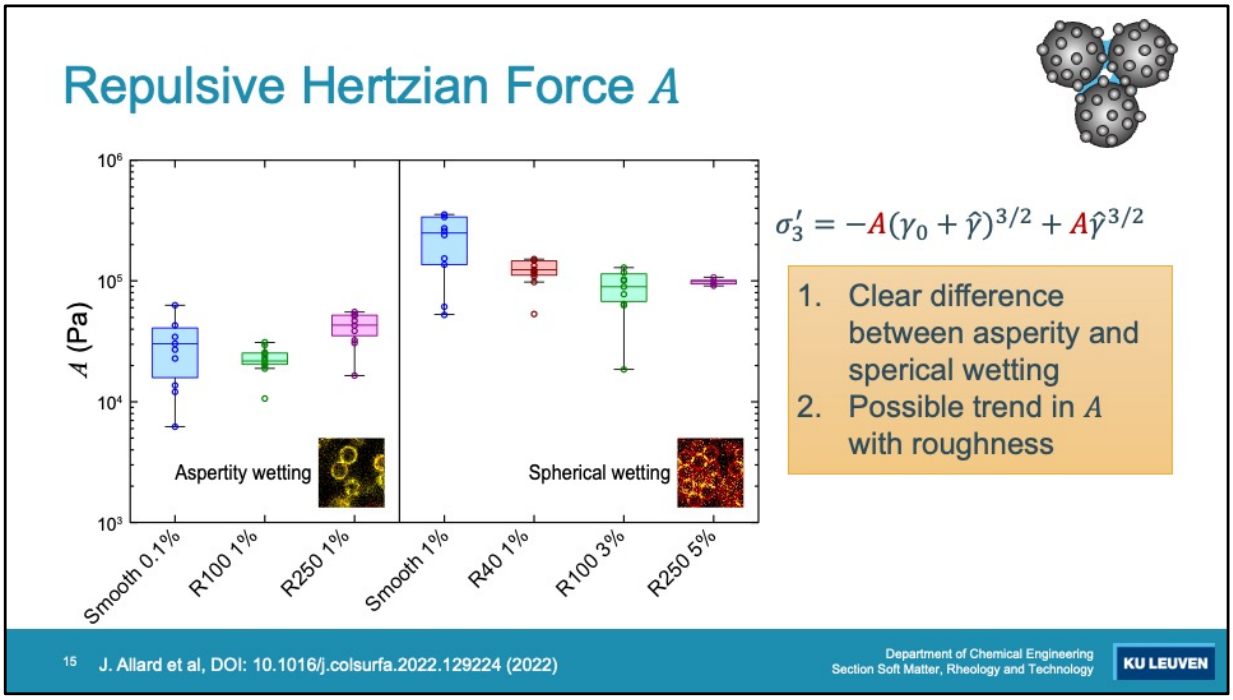

We hypothesize that the elastic scaling should be related to a combination of the capillary force, which brings the particles into contact, and the repulsive Hertzian contact force. The combination of these forces is given by the Johnson-Kendall-Roberts (JKR) theory

$$F = -\frac{4}{3}4E^* R^{1/2}\delta^{3/2} + 4\pi\Gamma R\left(1 + \frac{\delta}{4r}\right)$$

where E^* is the effective elastic modulus $1/E^* = 2(1-\nu^2)/E$, the indentation depth is given by δ and the bridge principal radius is r. When considering the effect of this contact on our networks, we have two main complications. First, we must consider that we have a network and the stress will be an average over all bonds in the system. The second complication is that we are not measuring the stress (first harmonic), but the third harmonic, which only includes the nonlinear terms. Using the JKR model as a guide, we propose that the elastic scaling should follow $\sigma_3' = -A(\gamma_0 + \hat{\gamma})^{3/2} + A\hat{\gamma}^{3/2}$ with fitting parameters A, the strength of the Hertzian contact, and $\hat{\gamma}$, the preloading strain. This equation predicts a power law exponent of 1.5 for the scaling of σ'_3 in the limit $\gamma_0 \gg \hat{\gamma}$.

Interestingly, clear differences between the sample groups are obtained when the repulsive Hertzian contact parameter A is plotted. The magnitude of this repulsion is affected by the Young's modulus and the contact area, which in turn is affected by the magnitude of the capillary bridge force. Concentrating on the matched ϕ_{sec} samples, we can see that A is largest for the smooth particle capillary suspension with a slightly lower value for the three rough particle samples. This trend is remarkable

since their plateau storage moduli were equal within experimental accuracy. This implies that this MAOS fit can indeed be sensitive to the particle contacts.

Conclusion: influence of particle roughness

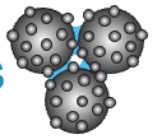

- Rheology-Structure
  - Moduli & yield stress: capillary suspension > pure suspension
  - ↑ ϕ_{sec}: more/larger bridges, ↑ strength (until funicular state)
  - ↑ Roughness: ↑ ϕ_{sec} needed, ↑ γ_{crit}, ↓ clustering
- Particle contacts: MAOS
  - 3rd harmonic scaling: non-integer, non-cubic
  - Transition from adhesion- to load-controlled friction?
  - Hertzian repulsion A: Pendular vs film bridging

arXiv preprint

16 J. Allard et al, DOI: 10.1016/j.colsurfa.2022.129224 (2022)

Department of Chemical Engineering
Section Soft Matter, Rheology and Technology

KU LEUVEN

Using a combination of oscillatory rheology and confocal microscopy measurements, we have shown that particle roughness influences the capillary force in capillary suspensions leading to changes in structure. With increased roughness, a higher wetting liquid volume is required to fill the asperities on the particle surface. The capillary force increases when transitioning from asperity wetting to bridge wetting. Consequently, the shear moduli of capillary suspensions with toroidal bridges are larger and the LVE region is extended compared to asperity wetting samples. By increasing the secondary liquid volume for high roughness samples, the moduli can be matched to that of the smooth particles, but the critical strain is slightly higher in all rough particle measurements.

The influence of particle roughness was further examined using information obtained from the medium amplitude (or asymptotically nonlinear) oscillatory shear regime. The non-cubic and non-integer scaling of the third harmonic stress signals was confirmed here for smooth and rough particle capillary suspensions. The strength of the Hertzian contact A decreases with roughness when the samples transition from bridge to asperity wetting but increases to similar values for the samples where the secondary fluid volume is adjusted to provide for pendular bridges. The ratio of the elastic to viscous scaling is tied to the nature of the frictional contact and a transition from adhesion- to load-controlled friction may occur in rougher samples. Our initial measurements point to such a transition, but additional measurements must be conducted.

Rheo-Confocal setup

Simultaneous imaging and rheology

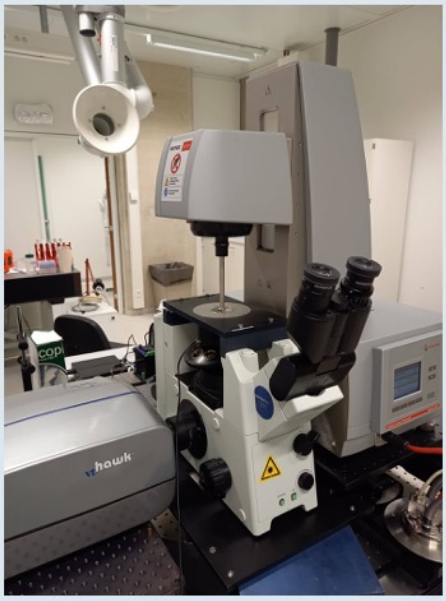

Department of Chemical Engineering
Section Soft Matter, Rheology and Technology
KU LEUVEN

One key objective this year was the creation of a rheo-confocal setup that we could use to study the dynamic changes the the capillary suspension networks.

Rheoconfocal setup

- MCR302 WSP rheometer + Zaber rails
  - Image between side and middle of geometry (up to 50 mm)
- VT-HAWK multi-beam confocal
  - Piezo actuator on objective for Z-scanning
- Cameras
  - Hamamatsu camera
    - Full field of view
    - 30 fps in 2D or 10 fps in 3D
  - High-speed camera
    - Up to 1000 fps
- Sapphire glass bottom plate
  - Slip can be an issue
  - Window bends a few µm at high normal load (e.g. rigid samples)

Department of Chemical Engineering
Section Soft Matter, Rheology and Technology
KU LEUVEN

This setup consists of an Anton Paar rheometer mounted to a fast-scanning multi-beam confocal microscope. The rheometer is mounted to a rail system to position the geometry so various positions between the edge and center of the geometry (up to 50 mm) can be imaged. The confocal includes two camera. The Hamamatsu camera is able to image the full field of view at up to 30 fps in 2D or 10 fps in 3D. There is also a high speed camera that can image up to 1000 fps, but the image intensity is currently insufficient to allow operation at the full speed. An upgraded camera with better image intensifier should fix this problem.

The lower geometry of the rheometer consists of a sapphire glass window. Sapphire glass is chosen for its mechanical (high stiffness reducing the thickness of the window, allowing a deeper field of view into the sample, while the hardness limits scratching of the window by silica particles) and optical (high transmissibility for large range of wavelengths) properties. Despite the stiffness, the window can bend a few µm under high normal load. This can be a problem during loading for rigid samples (such as the capillary suspension networks) since the subsequent relaxation or flexure of the window can move particles outside of the imaged plane (similar order of magnitude as the particle diameters). Pre-shearing of the sample has shown to reduce this problem. The smoothness of the window also presents a possible problem due to slip between the sample and the stationary lower plate.

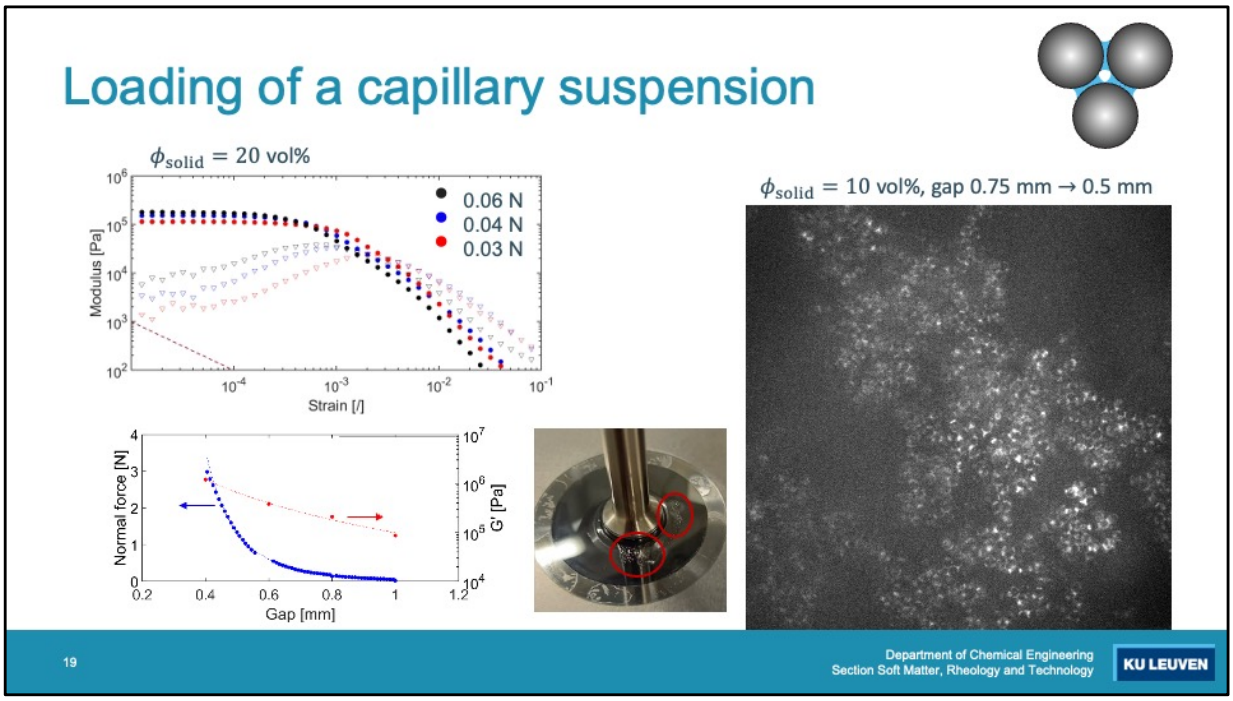

We previously observed a shift in the shear moduli towards higher values with loading at higher normal forces, as shown on the left for a $\phi_{\mathrm{solid}} = 20$ vol% sample. At a constant gap setting speed, the normal load increases dramatically as the gap decreases. This implies that the network compacts under the vertical load.

This is indeed what we see as we deform the experiment on the rheo-confocal setup. As we change the gap from 0.75 mm to 0.5 mm, we can see the deformation of the network. This deformation highlights the presence of larger flocs, each with a high packing, that appear to exhibit a type of rigid motion. These flocs shear past each other with only little internal rearrangements. These flocs might correspond to the glassy clusters predicted by Whitaker et al. (*Nat. Commun.* 2019, 10:2237). As the gap decreases, the solid loading increases as bulk liquid is expelled from the sample. This higher effective loading is the cause for the increasing normal force and shear moduli.

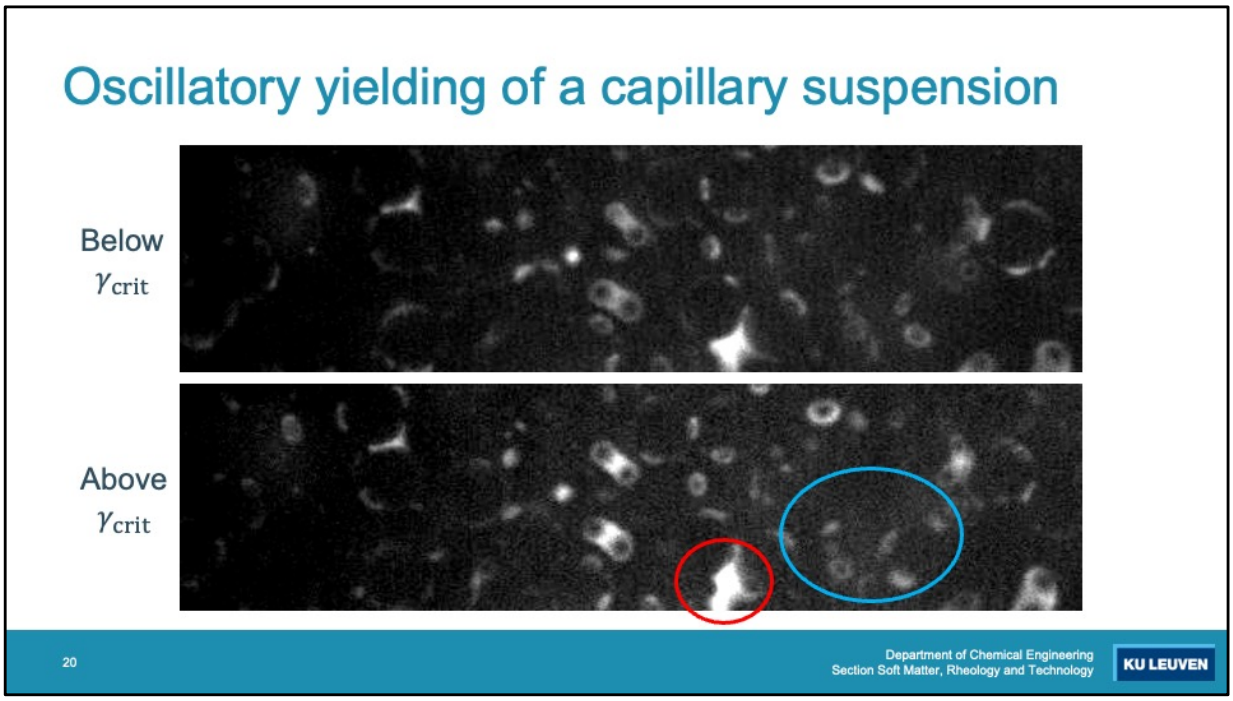

We can also perform experiments at increasing oscillatory amplitudes. For a smooth particle suspension, we can see a transition from the behavior below γ_{crit} where the particle network oscillates back and forth without any rearrangements and the behavior above γ_{crit} where rearrangements are observed. Here, we are just showing the secondary fluid channel. Here, we are highlighting two particle such events. In the red circle, a coalesced bridge connects a small cluster of particles. First, we see the lower part of this bridge breaking, excluding the lower particle. The bridge then migrates to the center of a particle pair where it stretches with the subsequent oscillations. In the blue region, a particle pair, connected to each other and several other particles by toroidal bridges, undergoes a slight rotation and movement in the focal axis.

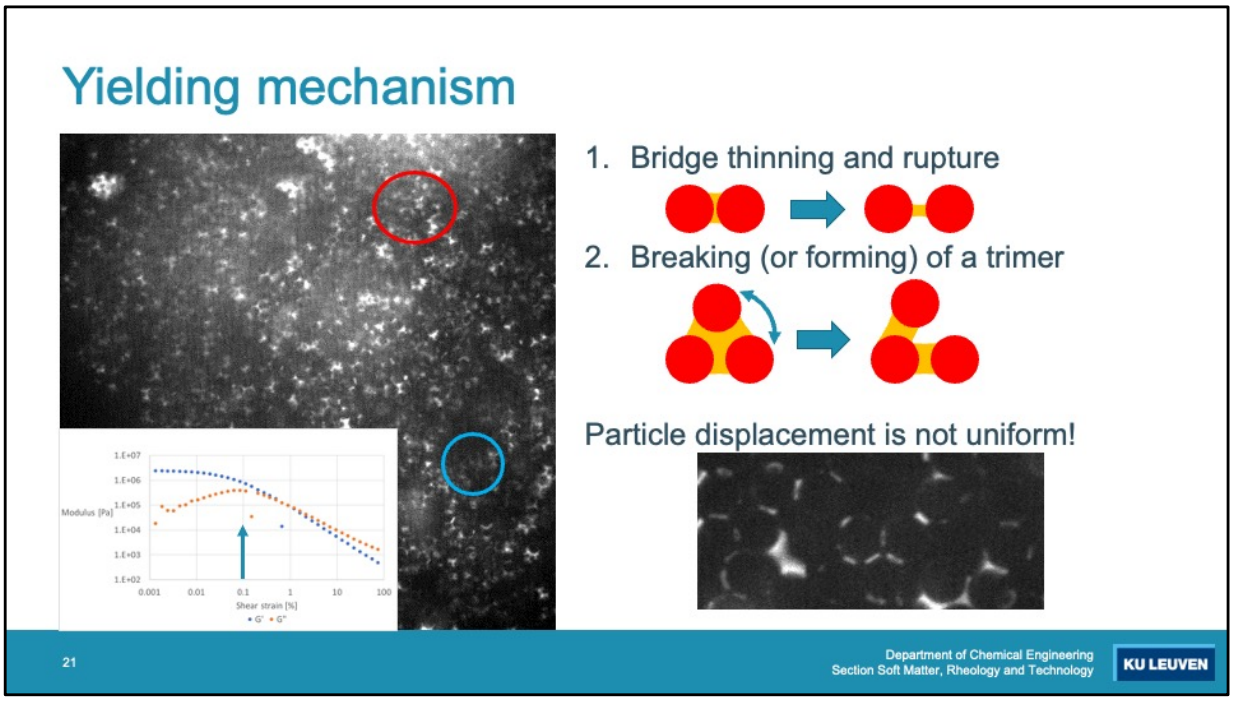

If we oscillate the sample at a single amplitude above the LVE, but below the flow point (indicated with the arrow), we see that despite macroscopic yielding, only a few particle rearrangements are visible in the imaged plane. In the video, we first see a bridge break and the secondary liquid migrate in the red region and then a trimer forming in the blue region. This highlights how yielding is highly localized and dependent on the local forces between particles. For example, if we zoom into a small region of the sample, we can see that most of the particles maintain their relative positions. It's only in the center of the image where the bridges stretch and particles rotate and stretch relative to their neighbors.

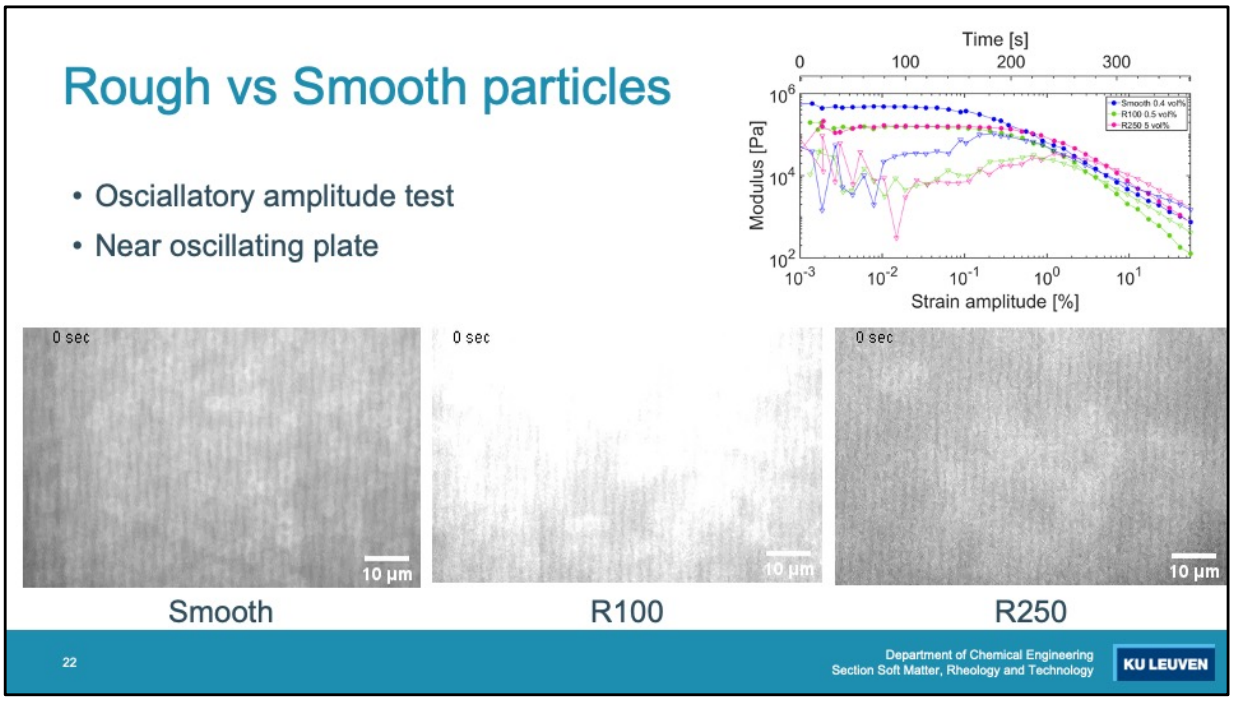

The increased resistance to particle movement due to the roughness is qualitatively confirmed by preliminary experiments with the rheo-confocal. These videos show the image plane close to the moving rheometer plate during amplitude sweeps. For the smooth particles, rearrangements of individuals particles happen before the G'' peak whereas rearrangements for the rough particles only occur after the G'' peak and usually occur in the form of rearrangements of small clusters rather than individual particles.

I should note that the image quality here, unfortunately, poor. While we can still see the movement, it's not possible to precisely track the particles here. There are a few reasons for this loss in quality.

1. Deep location within the sample. These images are taken near the moving rheometer plate (gap of 100 µm). A slight index of refraction mismatch between particles, secondary fluid, and bulk causes scattering in both the laser and emitted light and a loss of intensity. Typically, we are limited to image depths less than several hundred micrometers due these errors.
2. Alignment of the confocal and camera. Errors in the angle of the incoming laser (carried on a fiberoptic cable), confocal box, and camera can cause bright or dark spots in the image as well as the vertical lines shown in the image. This is currently being fine-tuned to improve the image quality.
3. Light intensifier. The intensifier, used to increase the photon count, particularly for high-speed images, has been damaged due to previous overexposure. The manufacturer has recommended an alternative system

with combined intensifier and camera. This will be implemented soon.

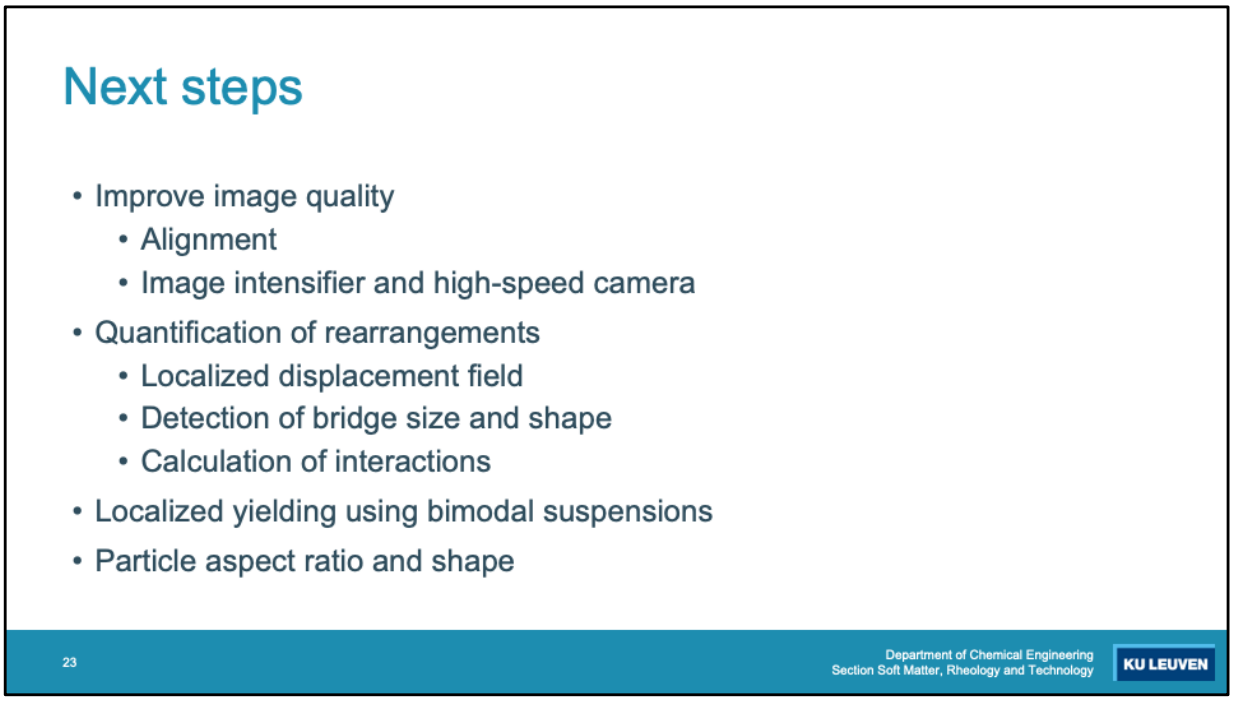

As just discussed, we are currently working to improve the image quality of the rheo-confocal images. This will soon allow us to quantify the rearrangements in the sample. This will include a quantification of the local displacement field (change in particle positions) as well as detection of the bridge size and shape. Using this bridge detection, we can then begin to calculate the interactions between particles and reconstruct force chains in the network. In the continuation of the project, we will also use bimodal suspensions to localize the yielding of the network. A low fraction of small particles in a large particle network (size ratio 1:3) can drastically weaken the network, because these bridges have a lower absolute capillary force and rupture distance. Confocal imaging is always limited to a small field of view. While the general structure in the field of view (usually on the order of 100 µm) may be representative of the bulk (mm to cm), yielding is highly localized. This means that the location of the first yielding event can be anywhere in the sample and most likely outside of the observed area. These initial yielding events can occur seconds or minutes before bulk yielding and changes that occur later in the observed area can lead to false hypotheses. By localizing the yielding events, we can pre-determine the location of yielding and study this mechanism in more detail.

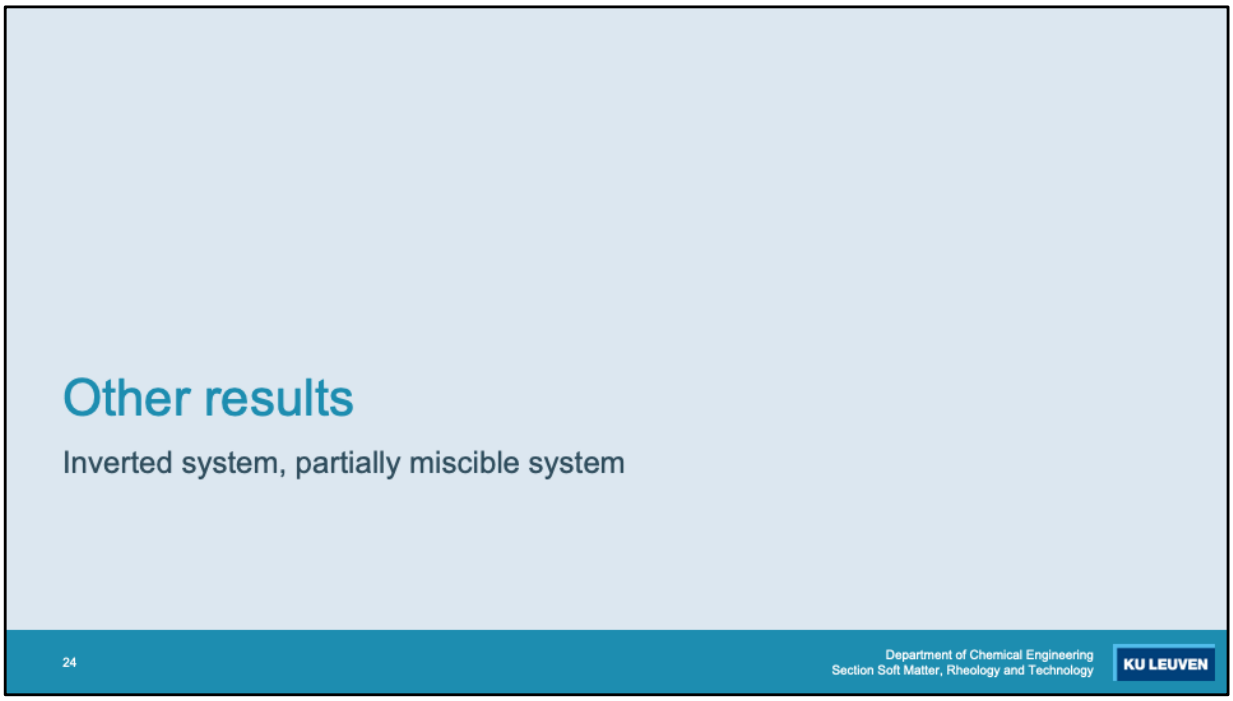

We also wanted to highlight a few other results from this year on an inverted system and on the partially miscible system.

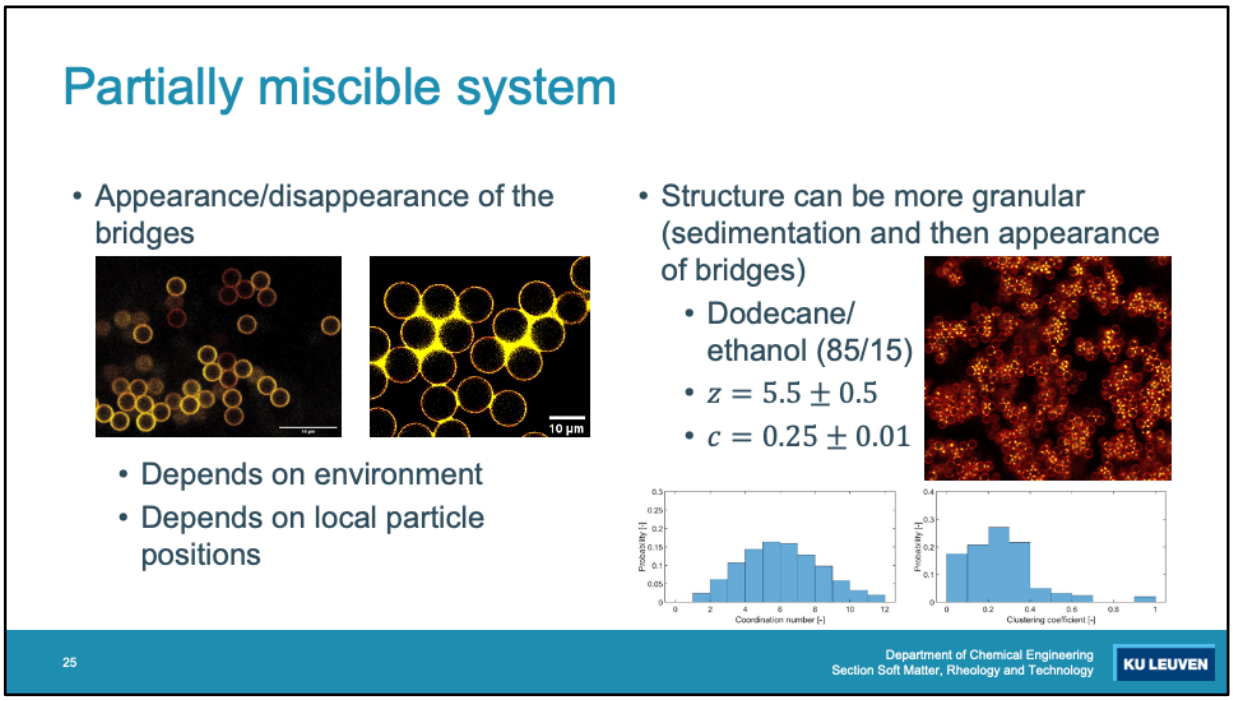

First, we continued the experiments with partially miscible liquids as part of a master thesis project this year. The student observed the appearance and disappearance of the bridges depending on the environment and local particle positions. For example (left video), when the local humidity is low, aqueous bridges can appear when the particles are added to the system and then disappear as the aqueous phase is transported through the bulk to the external environment. A difference is also observed between closed and open vessels. Particle separation (right video) influences break-up of the quadrimers (burst in the center of two trimers or collapse in the middle, in other words making 5 or 4 bridges).

In general, the partially miscible system results in a very uniform bridge size distribution, as shown in the right. However, the structure can be more granular since the particles tend to separate before the bridges form. This doesn't necessary equate to a more compact structure, however. For example, the dodecane/ethanol (85/15) system has a higher effective solid loading, but lower coordination number ($z = 5.5 \pm 0.5$) and clustering coefficient ($c = 0.25 \pm 0.01$) than the funicular hexamoll dinch/glycerol (97/3) system ($z = 6.1 \pm 0.1$, $c = 0.46 \pm 0.01$).

Nanoparticles incorporated into the bridges

- Lower G', longer LVE with increasing ϕ_{NP} in bridges ($\phi_{sec} = 1$ vol%)

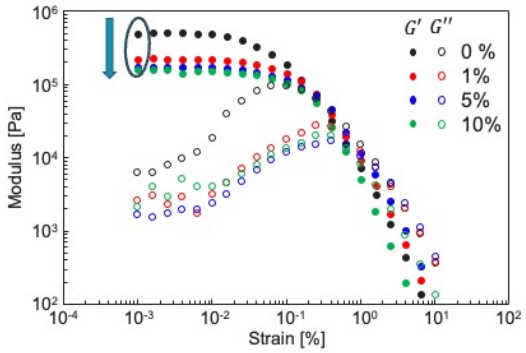

- No change in contact angle

$\phi_{NP} = 0$ $\phi_{NP} = 15$ vol%

- Change in wetting

$\phi_{NP} = 0$ $\phi_{NP} = 10$ vol%

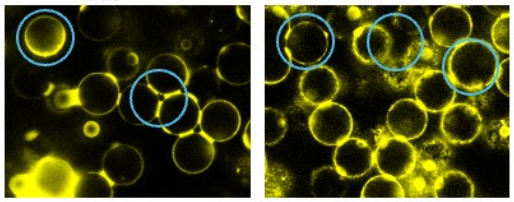

26

Department of Chemical Engineering
Section Soft Matter, Rheology and Technology
KU LEUVEN

Second, we've also been working with nanoparticles incorporated into the secondary fluid bridges as part of an EU funded project. Here, we see that adding increasing fraction of 16 nm fumed silica to the secondary fluid bridges ($\phi_{sec} = 1$ vol%) results in a lower shear moduli. The change in G' isn't linked to a change in the contact angle, but may be linked to a change in the wetting behavior. Without nanoparticles, the secondary fluid perfectly wets the particles and we have symmetrically distributed concave bridges. With 10 vol% silica in the bridges, we have uneven wetting and asymmetric bridges. Furthermore, there are clusters of nanoparticles observed on the microparticle surface that may be pinning the contact line. Despite these often smaller bridges, we have an extension in the critical strain marking the end of the LVE. This may be due to a different bridge breaking behavior and will be investigated using the rheo-confocal setup.

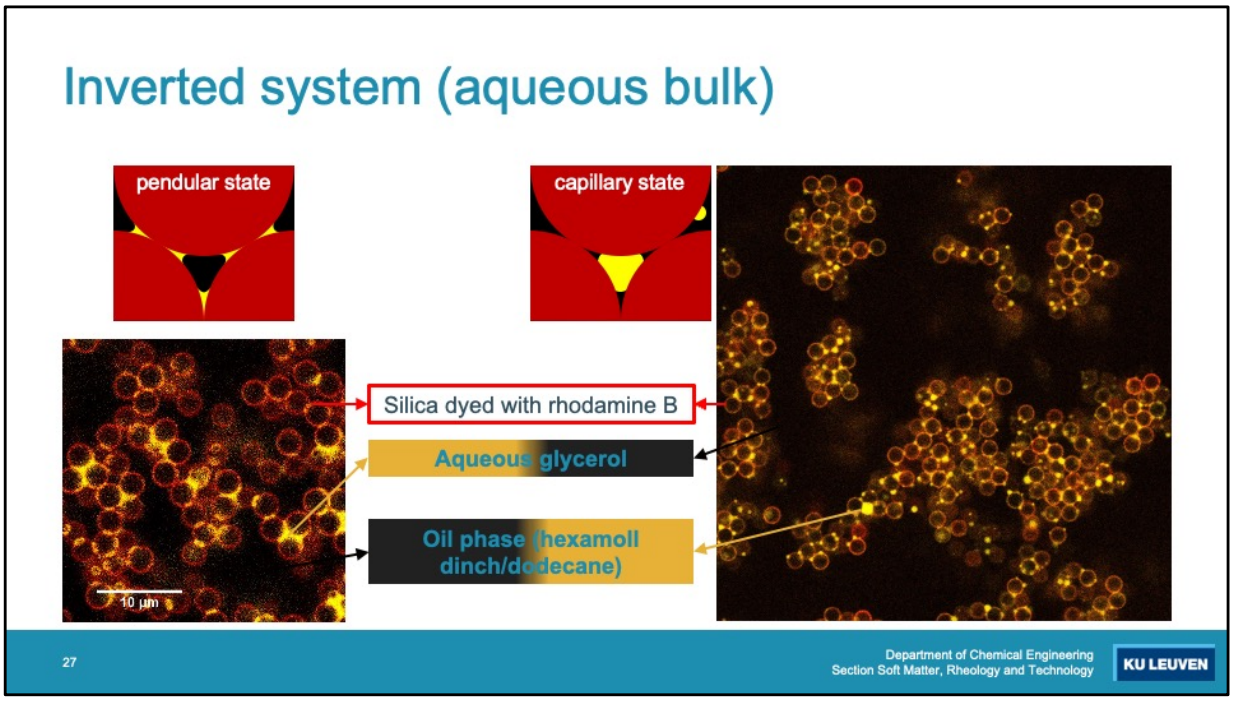

Finally, we have started to also do some experiments on an inverted system. Typically, we make our capillary suspensions with the oil phase (hexamoll dinch/dodecane) as the bulk fluid and aqueous glycerol as the secondary (bridging) liquid. With hydrophilic particles, the system is in the pendular or funicular state where the secondary fluid preferentially wets the bridges ($\theta < 90°$) and pendular bridges or trimers are formed. To create a capillary suspension in the capillary state, we typically hydrophobized the particles so that the contact angle $\theta > 90°$. We've also recently experimented with switching the bulk and secondary liquids. Previously, we found that the inverted system was unstable; it either formed weak Pickering emulsions or phase separated within a few minutes. Now, we've tried a neutrally wetting system with $\theta \approx 90°$. As shown on the right, these neutrally wetting particles are able to form a capillary state suspension when the particles are added to the pre-emulsified liquids. While initially a curiosity to see if we could invert the system, this may be an interesting path for future research.

Thank you for your attention!

Department of Chemical Engineering
Section Soft Matter, Rheology and Technology
KU LEUVEN